

Revealing the Accelerated Capacity Decay of a High-Voltage LiCoO₂ upon Harsh Charging Procedure

Zijian Li, Haocong Yi, Wangyang Ding, Hengyu Ren, Yuhao Du, Mingjie Shang, Wenguang Zhao, Hui Chen, Lin Zhou, Hai Lin, Qinghe Zhao,* and Feng Pan*

In practical applications, LiCoO₂ (LCO) cathode is usually charged with a constant current plus constant voltage (CC+CV) procedure to obtain higher capacity delivery. However, the harsh condition upon CC+CV procedure causes the accelerated capacity decay of LCO. Herein, the fading mechanism of LCO cycling upon CC+CV procedure at 4.6 V versus Li/Li⁺ is first revealed. Comparing with a pure CC charging, the accelerated capacity decay of LCO upon CC+CV procedure is attributed to both the bulk and surface structure damages: i) the CV charging triggers more H1-3 phase separation, leading to the generation of lattice dislocations, curved Co-O layers, and ultimately the bulk microcracks inside the LCO particles; ii) upon cycle, the CV charging causes more side reactions and more surface structure collapse issues, including forming thick surface phase transition layer (PTL), causing more Co dissolution, forming thick and loose CEI layer, etc., which seriously increases the charge transfer resistance and reduces the interface Li⁺ transport kinetics. This work provides a new insight into the fading mechanism, and shows a new pathway for designing more advanced LCO cathodes.

1. Introduction

For past decades, the Li-ion batteries with LiCoO $_2$ (LCO) as cathodes have been the most widely used batteries in the portable devices, mainly due to the advantages of high compact density and long cycle stability. However, in practical applications, LCO cathodes can usually provide an insufficient capacity due to the low operating voltage. For example, when operated at 4.45 V versus Li/Li $^+$, LCO can only provide \approx 170 mAh g $^{-1}$, resulting in an inferior energy density. To achieve higher energy density, increasing the charging cut-off voltage of LCO is an effective method. For example, when the cut-off voltage is raised to 4.6 V,

Z. Li, H. Yi, W. Ding, H. Ren, Y. Du, M. Shang, W. Zhao, L. Zhou, H. Lin, Q. Zhao, F. Pan

School of Advanced Materials

Peking University Shenzhen Graduate School

Shenzhen 518055, China

E-mail: zhaoqh@pku.edu.cn; panfeng@pkusz.edu.cn

H. Chen

School of Materials and Environmental Engineering Shenzhen Polytechnic Shenzhen 518055, P. R. China

D

The ORCID identification number(s) for the author(s) of this article can be found under https://doi.org/10.1002/adfm.202312837

DOI: 10.1002/adfm.202312837

LCO can release a capacity of \approx 220 mAh g⁻¹, which is \approx 135% of energy density of LCO at 4.45 V.^[4]

Despite the higher capacity at highvoltage, the serious irreversible structural damages due to more Li+ ion's removal block the practical applications of LCO. Generally, when charged to beyond 4.55 V, the O3 phase of LCO undergoes a gradual phase transition toward H1-3 phase or even O1 phase,^[5] which causes serious lattice shrinkage and large internal stress inside the LCO particles, and accumulates into cracks and even particle pulverization upon cycle.[6] Comparing with the bulk structural damage, the surface structure issue is more serious when charged to voltages beyond 4.55 V. On one hand, the highly oxidative lattice Co⁴⁺ and O^{α -} (α <2) on LCO surface can trigger more side reactions to form cathode electrolyte interface (CEI) layers with poor protective ability; on the other hand, the O release and Co dissolution from

the surface structure can lead to the appearance of disordered phases with poor ion conductivity.^[7] As a result, the Li⁺ ion's transport across the surface structure is seriously blocked, leading to a rapid capacity decay.

Revealing the fading mechanisms is significant to guide the design of the more advanced LCO materials. However, in practical applications, the batteries are used in different application scenarios, including under the conditions of room temperature,[8] high temperature, [3b,9] over-charged, [10] over-discharged, [10a,11] floating charged, and rolled with high roll pressure, [9b,12] etc. The differences among the above scenarios lead to the different fading mechanisms. For example, Tan et al.[8] has reported the gliding of Co-O slabs upon high voltage can lead to the irreversible structural transition, leading to the formation of some Li⁺-ion blocking phases, including both the spinel (Co₃O₄ or Li_{1-x}Co_{2+x}O₄) and rock-salt (RS, CoO) phases on the surface region. Aurbach et al. [9a] have revealed that the generation of high resistance and thick CEI is responsible for the capacity decay under high temperatures, such as cycling/storage in the LiPF₆/alkyl-carbon electrolyte system under 45 and 60 °C. The previous report of our team contributes the deteriorated structure stability of LCO at 45 °C to the triggered side reactions and the blocked Li⁺-ion transport channels.^[13] Yan et al.^[9d] have not only proposed that the high catalytic activity of Co⁴⁺ sites on the surface of LCO at high temperatures (i.e., 55 °C), which could

www.afm-journal.de

1616208.2, 2024, 14, Downloaded from https://advanced.onlinelibrary.viely.com/doi/10.1002/adrff.202312897 by University Town Of Shenzhen, Wiley Online Library on [2311/2025]. See the Terms and Conditions (https://onlinelibrary.wiley.com/terms-and-conditions) on Wiley Online Library or rules of use; OA articles are governed by the applicable Creative Commons License

promote the electrolyte decomposition, but also found the loss of lattice O and the migration of metal (TM) ions from the octahedral positions in TM layers to the tetrahedral positions in Li layers at elevated temperatures. By observing the macroscopic/ microscopic morphology results of LCO upon overcharging, Oh et al.[10c] have elucidated that the overcharging can lead to the appearance of heterogeneous phases (spinel/RS phases) in the bulk and abnormal cracking near the heterogeneous phases. Sun et al.[11] have found that the obviously decreased electronic/ionic conductivity of the newly emerged Li₂CoO₂ phase on surface of LCO is responsible for the capacity decay under the overdischarged conditions. Hirooka et al. [9b,12b] have studied the relationship between structural degradation and capacity decay of LCO under high-temperature float charging (60 °C/4.4 V) in the graphite/LCO cells. They proposed that the capacity fading of LCO was mainly due to the disproportionation of the charged LCO into Co²⁺ and CoO₂ with O1 phase under when exposed to HF-containing circumstances. Besides, the fading mechanism caused by grain boundary cracking (GBC) inside LCO particles has also been revealed by our group.^[14] It was found that the excessive rolling stress could cause the GBC formation inside a polycrystalline LCO, forcing cracks to extend along grain boundaries in the bulk, exposing new interfaces to the electrolyte, and leading to irreversible damage to the bulk structure.

Herein, for the first time, we reveal the accelerated capacity decay of LCO upon a harsh charging condition, that is, upon a constant current plus constant voltage (CC+CV) charging, which is rarely reported in previous literatures. Since the CC+CV charging procedure is frequently utilized in industry, revealing the correlated fading mechanism provides significant guidance for designing the more advanced LCO cathodes. A high-voltage LCO is achieved mainly via constructing a surface Al/F enriched RS layer, and is used to study the fading mechanism upon CC+CV charging procedure. The results clearly show that, the cyclic CV charging not only leads to severe bulk structure deterioration, but also triggers more side reactions and results in the generation of surface high resistance heterogeneous phase layers on the surface region. The detailed analyses are systematically illustrated in the following sections. We hope that the obtained results in this work can provide some clues for the development of the nextgeneration LCO cathodes.

2. Results and Discussion

2.1. Characterization of a High-Voltage LCO

As reported in the previous reports, [7b,15] the surface Al/F decoration can play a beneficial role on enhancing the cycle performance of LCO. Therefore, to obtain a reinforced cycle stability, we perform a Al/F coating on a commercial LCO, via simply mixing and grinding the AlF₃, LiF, and LCO powders, then following with an sintering process at 600 °C in air atmosphere. The detailed method is illustrated in Supporting Information. The obtained LCO with Al/F coating is named as AF-LCO, with a median diameter (D_{50}) of \approx 4.5 µm. Figure 1a shows the scanning electron microscopy (SEM) morphology and elemental distributions of the AF-LCO with Al/F enriched surface, indicating a uniformly distributed Al/F elements on LCO surface. The phase structure of LCO is analyzed through X-ray diffraction (XRD) method, and the XRD refinement is also conducted, as shown in Figure 1b. The result shows a typical R-3m phase structure of LCO, indicating that the Al/F coating shows nearly no influence on the bulk structure of LCO, but to reinforce the toughness of surface structure.

In order to probe the surface structure variation upon Al/F coating, the transmission electron microscopy (TEM) and corresponding fast Fourier transform images (FFT) are conducted. Figure 1c clearly shows phase structures of both the surface and subsurface regions of LCO. It is noted that, an obvious RS phase layer with a thickness of $\approx 1-3$ nm is observed in the outermost surface, illustrating that the Al/F coating can promote the phase transitions from layered to RS structure, which is thermodynamically more stable against the corrosive surface circumstances upon a high voltage of 4.6 V.[8,16] Besides the outermost surface RS phase layers, the surface structure in the deeper area (region B) still remains a layered structure.

The X-ray photoelectron spectroscopy (XPS) is further performed to detect the surface chemical forms of Al and F on the surface, as shown in Figure 1d, which shows the fine spectra of both Al 2p and F 1s. For the F 1s spectra, the two peaks locating at ≈685.8 and 685.0 eV are attributed to the peaks of Li-Al-F and LiF, respectively.[15a] For the Al 2p spectra, the peaks locating at ≈76.0 and 73.0 eV represent the presence of Al-F and LiCo_{1,v}Al_vO₂, respectively.^[17] As the etching depth increases, the peak of LiF diminishes, indicating that LiF is enriched mainly on the outermost surface of AF-LCO, acting as a prefabricated artificial CEI layer. Besides, it is noted that the presence of Li-Al-F, Al-F, and LiCo_{1,x}Al_xO₂ always appear upon etching, indicating that the Al and F can penetrate to the lattice framework in the surface region upon sintering at 600 °C. After all, a high-voltage LCO with a tough Al/F enriched RS layer is successfully synthesized with enhanced cycle stability based on commercial high-voltage electrolyte, which will be utilized to explore the fading mechanism under a constant current plus constant voltage (CC+CV) charging procedure.

2.2. Deteriorated Cycle Stability

Figure 2a shows the illustration of the CC+CV charging and CC discharging procedure, that is, one charge/ discharge cycle of the LCO cathode involves first charging to 4.6 V with a constant current of i_0 , then continuing to charge at a constant voltage of 4.6 V until to a cut-off current of i_1 , and then the LCO cathode is discharged with a constant current of i_2 . Herein, the AF-LCO/Li half-cells are assembled and tested to explore the influence of the cut-off currents of CV charging on electrode cycle stability of AF-LCO, and the active loading of AF-LCO electrode is \approx 6 mg cm⁻². Figure 2b compares the cycle performances of the AF-LCO/Li half-cells with different cut-off currents of CV charging. The currents for both CC charging (i_0) and CC discharging (i_2) are designed as 1 C (1 C = 200 mA g^{-1}), and the cut-off currents of CV charging (i₁) are 0.5 C, 0.2 C, 0.1 C, 0.05 C, and 0.02 C, respectively. A pure CC charging/ discharging procedure equals to the CC+CV procedure with a cut-off current of 1C. It can be noticed that, the AF-LCO/Li cells show initial capacity deliveries of 209.2, 210.0, 215.3, 219.9, 221.9, and 223.6 mAh g⁻¹ at the cut-off currents of 1 C, 0.5 C, 0.2 C, 0.1 C, 0.05 C, and 0.02 C, respectively,

16163028, 2024, 14, Downloaded from https://advanced.onlinelibrary.wiley.com/doi/10.1002/adfm.202312837 by University Town Of Shenzhen, Wiley Online Library on [23/11/2025]. See the Terms

onditions) on Wiley Online Library for rules of use; OA articles are governed by the applicable Creative Commons

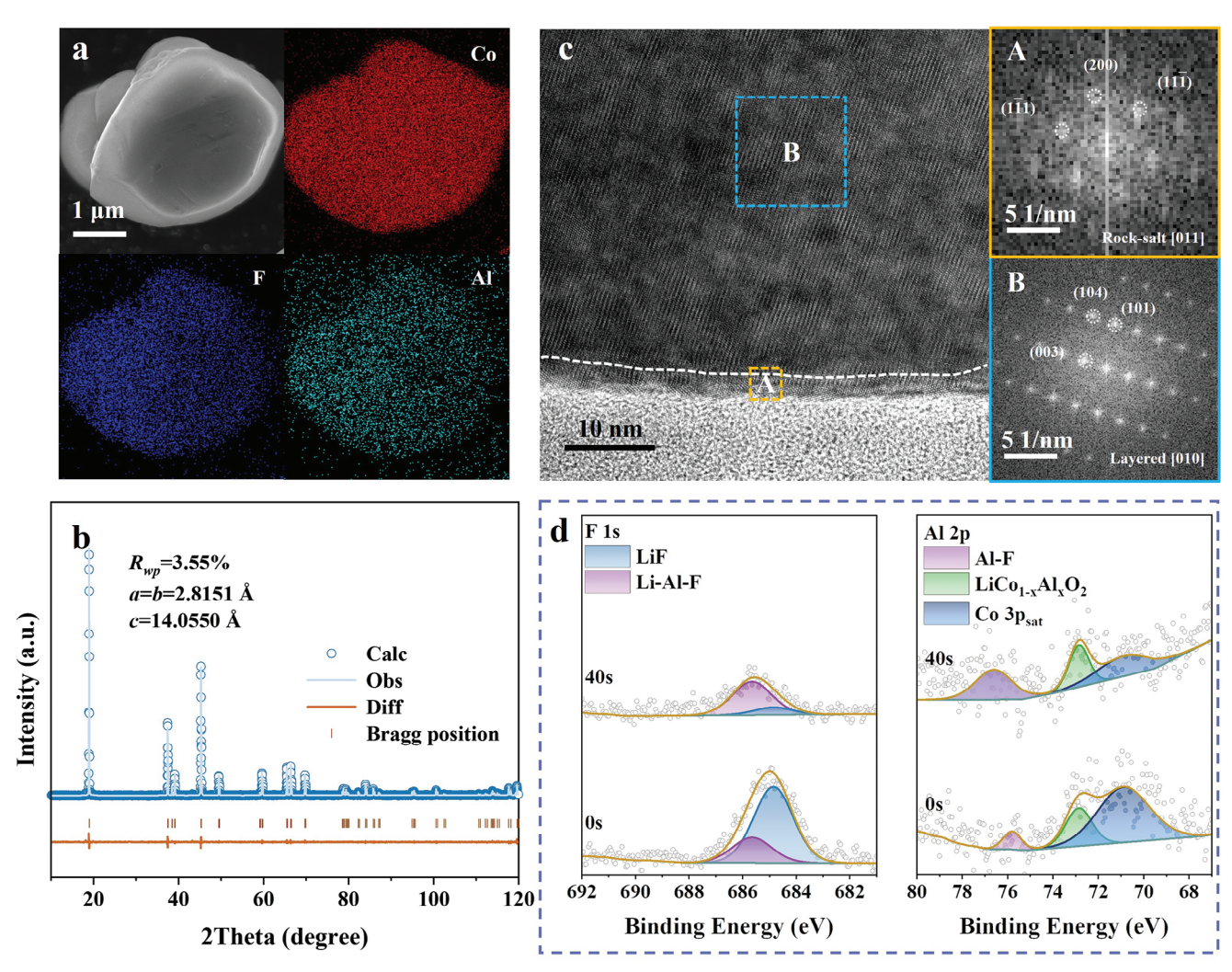


Figure 1. Material characterizations of AF-LCO. a) SEM morphology and corresponding EDS-mapping results of AF-LCO. b) TEM characterizations of the surface/bulk structures of AF-LCO. c) XRD refinement result of AF-LCO. d) XPS analyses of F 1s and Al 2p spectra results.

indicating the elevated capacity deliveries due to the CV charging. However, as the value of cut-off currents decreases from 1 C to 0.02 C, the capacity retention after 200 cycles reduces sharply from 92.4% to 54.5%, illustrating the adverse impact of the CV charging on cycle stability of AF-LCO/Li cells. Besides, we find that the AF-LCO/Li cell with a cut-off current of 0.2 C upon CV charging achieves a best balance between the initial capacity delivery and cycle stability, which is firstly reported in literatures. Specifically, upon this charging procedure, AF-LCO can deliver a reversible discharge capacity of 215.3 mAh g $^{-1}$ and a retention over 80% after 200 cycles.

Figure S1a (Supporting Information) compares the charging/discharging curves of AF-LCO/Li cells upon different CC+CV procedures at 5th, 100th, and 200th cycles, respectively. For cells with CC+CV charging procedures, the 5th discharge curves show a very obvious plateau of H1-3 phase transition to O3 at \approx 4.47 V.^[18] The dQ/dV curves shown in Figure 2c further prove that the peaks of H1-3/O3 phase transition become more pronounced with the decreased cut-off currents upon CV charging. As the cycle prolongs, the voltage polarization of AF-

LCO/Li cells shows an increasing trend linearly with the decreased cut-off current at CV charging procedure, after both the 100 and 200 cycles, as shown in Figure S1b,c (Supporting Information). Meanwhile, the dQ/dV curves in Figure 2d show that, the peaks representing the H1-3/O3 phase transitions at \approx 4.35– 4.55 V,[19] and the peaks representing the O3-I/O3-II phase transitions at $\approx 3.8-3.9$ V,^[20] become more irreversible with the decreased cut-off currents from 1 C to 0.02 C upon CV charging procedures. Specifically, after 200 cycles, the redox peak differences between the charging/ discharging plateaus reach 0.271 V for the cell with a low cut-off current of 0.02 C, which is much >0.0621 V for the cell operated under a pure CC procedure. Both the comparisons of charging/ discharging curves and the dQ/dV curves indicate the increased redox polarizations due to the decreased cut-off currents upon CV charging procedure. The increase in voltage polarizations can be further reflected in the median voltage curves upon cycle (Figure 2e). In summary, although applying CV charging can improve the capacity delivery, the cycle stability will be significantly reduced due to the obviously increased voltage polarization. The fading

16163028, 2024, 14, Downloaded from https://advanced.onlinelibrary.wiley.com/doi/10.1002/adfm.202312837 by University Town Of Stenzhen, Wiley Online Library on [23/11/2025]. See the Terms and Conditions (https://onlinelibrary.wiley.

-conditions) on Wiley Online Library for rules of use; OA articles are governed by the applicable Creative Commons

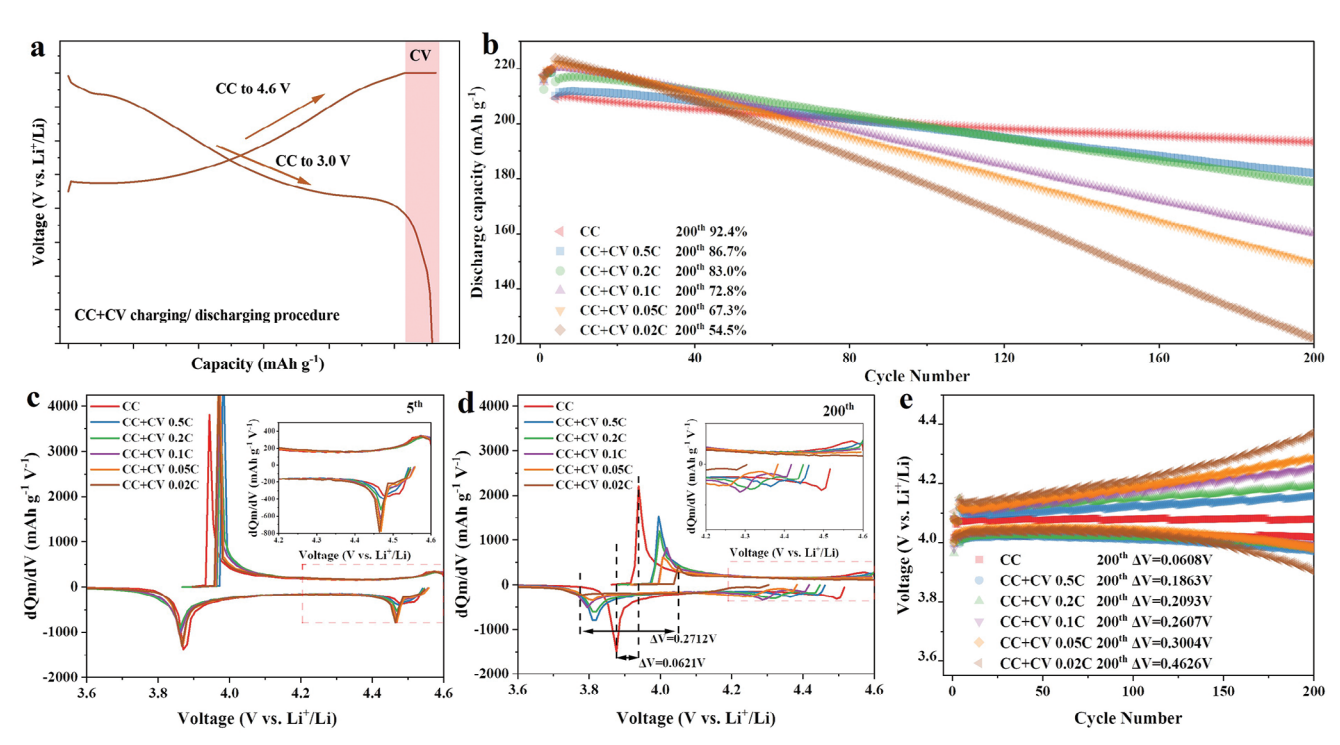


Figure 2. Electrode performances of AF-LCO/Li cells. a) Schematic illustration representing the CC+CV charging/discharging procedure. b) Comparison of cycle performances of AF-LCO/Li cells upon various CC+CV procedures with different cut-off currents from 1 to 0.02 C. c,d) Comparison of dQ/dV curves of AF-LCO/Li cells upon various CC+CV procedures after 5th cycle and 200th cycle, respectively. e) Comparison of the median voltage of AF-LCO/Li cells upon various CC+CV procedures.

mechanism of CC+CV procedure will be discussed in the following parts.

2.3. Phase Transformations and Microcrack's Generation

As discussed above, the CV charging in CC+CV procedure can induce the higher redox polarization of AF-LCO. In order to understand the underlying mechanism of this phenomenon, the in situ XRD characterizations are carried out to illustrate the phase evolution behaviors in the initial two cycles, and the AF-LCO electrodes are operated upon pure CC and CC+CV (with a cut-off current of 0.02 C) procedures, respectively (Figure 3a,b). Generally, the shift of the (003) peaks $\approx 19.1^{\circ}$ represents the change of the c-axis, and the sudden changes of the (101) planes $\approx 37.4^{\circ}$ indicate the glide of Co-O slabs beyond 4.55 V.[8] The interlayer spacing change caused by O1a phase is clearly illustrated in Figure S2 (Supporting Information). For AF-LCO operated upon pure CC procedure, when charged to 4.6 V, the (003) peak shifts to ≈19.25°, indicating the phase transition from O3 to H1-3 (mixed phases of O3 and O1). Notably, we notice that there is no obvious shift of (101) peak, indicating that the sliding of Co-O slabs does not occur, which may be related to the protection of surface modification by Al/F enriched RS layer. That is to say, the fewer H1-3 phase transition and lesser sliding of Co-O slabs contributes to the high cycle stability of AF-LCO cycling upon pure CC procedure.

In contrast, for AF-LCO electrodes operated upon CC+CV procedure, the cleavage of (003) peaks appears, which corresponds

well to the significant H1-3 phase separation upon CV charging. Specifically, there are two splitting peaks at $\approx 19.35^{\circ}$ and 19.71° , and the peaks at $\approx 19.71^{\circ}$ correspond to the O1a phase in H1-3, as shown in Figure 3c. As the CV charging proceeds, the proportion of O1a phase shows a remarkable increase, indicating more H1-3 separation and gliding of the Co-O slabs. Besides, the intensified gliding of Co-O slabs can be further evidenced by the sudden shift of (101) peaks upon CV charging. Figure 3d shows the XRD patterns of the AF-LCO electrodes at discharged states after 1st, 5th, and 200th cycles. For AF-LCO upon pure CC procedure, the (003) peaks maintain nearly no change in 200 cycles, while for AF-LCO upon CC+CV procedure, the (003) peaks show an obvious left shift in 200 cycles, indicating the severe phase structure damage due to the repeated H1-3 separation and gliding of the Co-O slabs. In addition, the peaks half-width of (003) planes upon CC+CV procedure also increase obviously at the 200th cycle, indicating the attenuation of crystallinity upon cycle, while for AF-LCO upon pure CV procedure, the (003) peaks show no significant changes.

SEM characterizations are further conducted to demonstrate the accumulation of irreversible structure damage of AF-LCO upon CC+CV procedure, as shown in Figure 4a–c. A vivid crack's generation process is identified via analyzing the SEM morphology of AF-LCO electrodes at the 1st, 50th, and 200th cycles, respectively. Slight cracks with a step-like morphology are observed on the surface of AF-LCO after the 1st cycle, and it gradually gains and becomes more severe after the 50th cycle, and eventually evolves into cracks across the entire particle after the 200th cycle. On the contrary, for AF-LCO upon pure CC procedure, there

16163028, 2024, 14, Downloaded from https://adv

anced.onlinelibrary.wiley.com/doi/10.1002/adfm.202312837 by University Town Of Shenzhen, Wiley Online Library on [23/11/2025]. See the Terms and Conditions

onditions) on Wiley Online Library for rules of use; OA articles are governed by the applicable Creative Commons

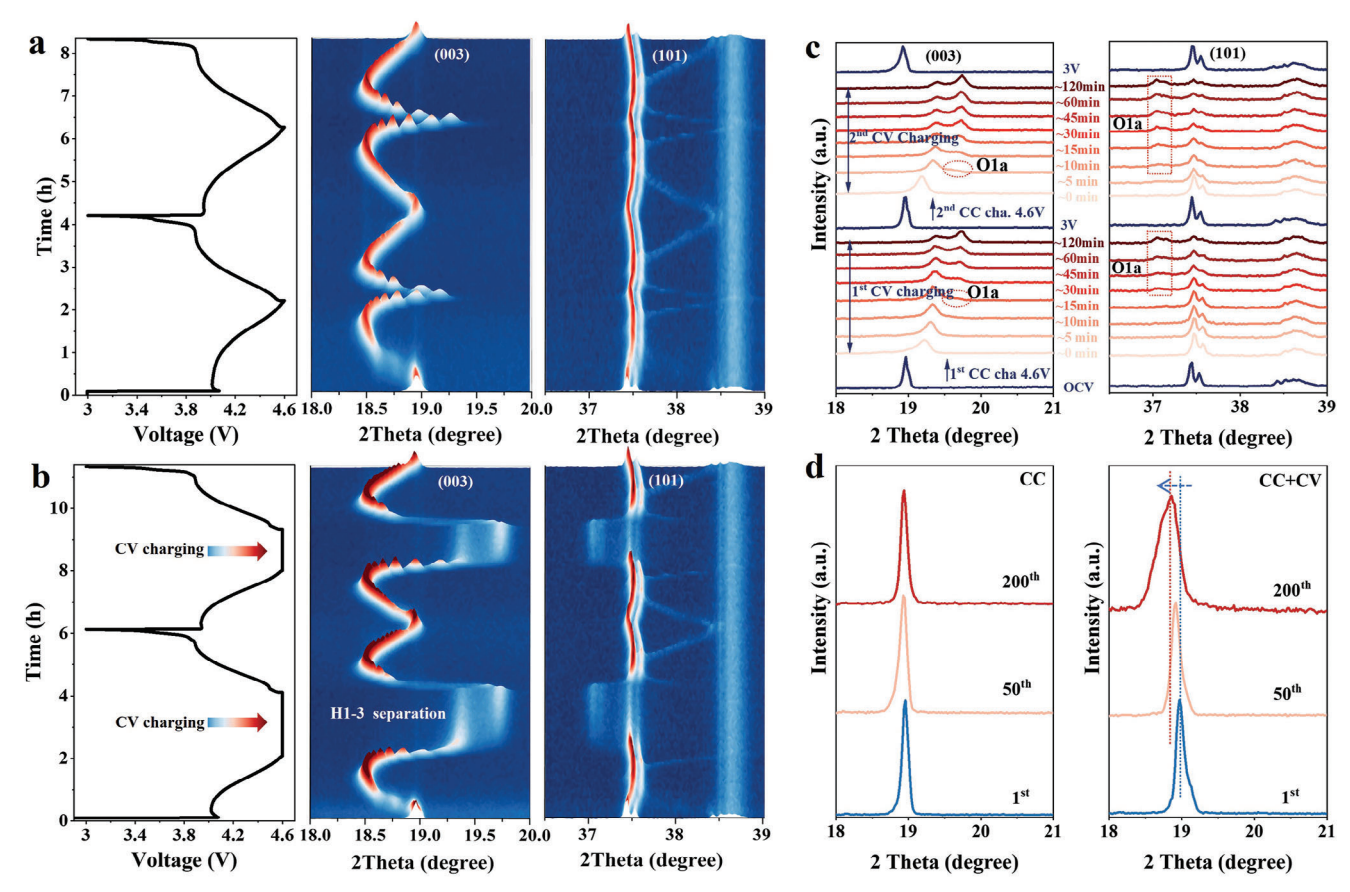


Figure 3. Bulk phase evolution of AF-LCO electrodes upon CC and CC+CV procedures. a,b) The in situ XRD patterns of AF-LCO electrodes in the initial two cycles upon pure CC and CC+CV procedures, respectively. c) The variation of (003) and (101) peaks of AF-LCO electrode upon CV charging process upon CC+CV procedure. d) Comparison of (003) peaks of AF-LCO electrodes after the 1st, 50th, and 200th cycles upon CC and CC+CV procedures.

are almost no obvious cracks after the 200th cycle (Figure S3, Supporting Information). The results indicate that, applying CV charging can induce more H1-3 phase separation and more gliding of Co-O slabs, which is regarded as the structure origin for the crack's generation. Once the cracks generate, some fresh Co-O surface will be exposed to the corrosive electrolytes, leading to more structure damage upon long-term cycles.^[21]

We further conduct the TEM characterizations to reveal the crack's generation in the bulk region of AF-LCO after the 50th and 200th cycles upon CC+CV procedure. After 50th cycle, some lattice dislocations are observed in the bulk region of AF-LCO (Figure 4d), accompanied with the appearance of some spinellike phases, as shown in FFT patterns. After the 200th cycle, the aggravation of lattice dislocations evolves to the severe local lattice disorder and curved Co-O slabs (Figure 4e), and the microcracks (Figure S4a, Supporting Information). Meanwhile, the proportion of the spinel-like phases gains, and the interlink between diffraction spots of layered phases appear, mainly due to the appearance of the massive discontinuous Co-O layers.^[22] In contrast, for AF-LCO upon pure CC procedure, the flat Co-O layers with clear diffraction patterns corresponding to the pure layered structure are observed after the 50th and 200th cycles (Figure 2d,e), and no microcracks are observed in the bulk region of AF-LCO (Figure \$4b, Supporting Information). We consider that, the severe structure damages induced by the repeated CV charging, including lattice disorders, curved Co-O layers, and microcracks, etc., which is one of the main reasons for the accelerated capacity decay of the AF-LCO.

2.4. Surface Structure Deterioration

Comparing with the bulk structure, the surface structure of LCO possess more delithiation upon charging, thus the surface structure deterioration issues have always been considered as the most prominent factor for the capacity decay.[23] After the 1st cycle, for AF-LCO upon CC+CV procedure, a phase transition layer (PTL) is observed on the surface region of AF-LCO, featuring a layer/spinel hybrid phase with thickness of ≈10 nm, while the subsurface region still shows a pure layered structure (Figure 5a). This result indicates that part of the layered LiCoO₂ can transform to the spinel-like Li_xCo₂O₄ upon charging.^[24] As the cycle proceeds, the thickness of surface PTL gains rapidly to ≈20 nm after the 50th cycle, and the subsurface structure also shows a little feature of layer/ spinel hybrid phase (Figure \$5a, Supporting Information), indicating the expansion of PTL from surface into interior. After the 200th cycle, not only the surface PTL expands to a disturbing thickness of beyond 50 nm, but also the Co-O

16163028, 2024, 14, Downloaded from https://adv

onlinelibrary, wiley, com/doi/10.1002/adfm.202312837 by University Town Of Shenzhen, Wiley Online Library on [23/11/2025]. See the Terms

conditions) on Wiley Online Library for rules of use; OA articles are governed by the applicable Creative Commons

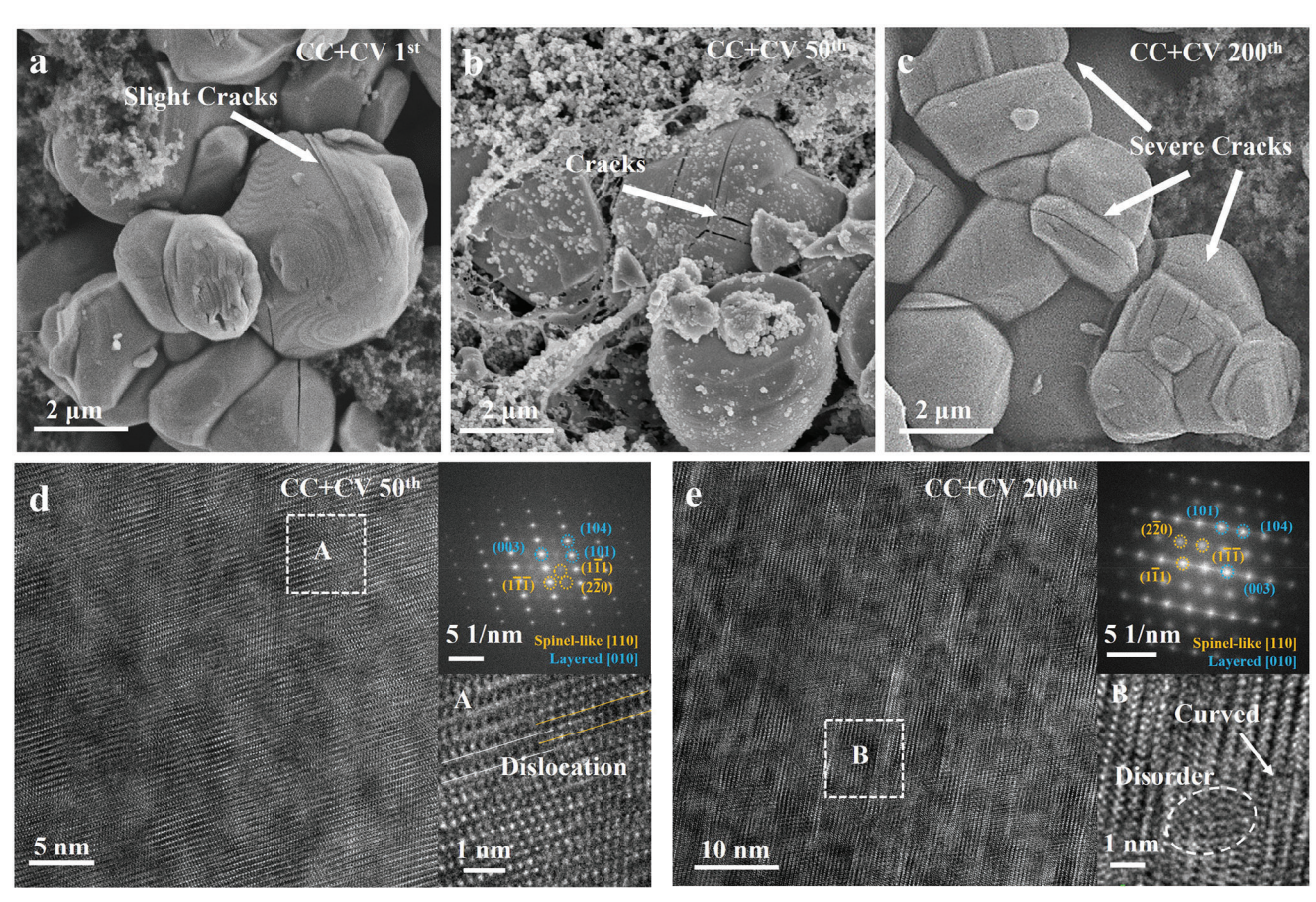


Figure 4. Crack's generation and bulk structure deterioration upon cycle. a-c) SEM morphologies to illustrate the crack's generation process of AF-LCO particles after the 1st, 50th, and 200th cycles. d,e) TEM characterizations of lattice dislocation after 50th cycle, and the lattice disorder and curved Co-O layers of AF-LCO upon CC+CV procedure after 200th cycle.

layers become more curved and discontinuous, as confirmed by the interlink between the diffraction spots, [25] as shown in Figure 5b, which acts as a big obstacle for Li⁺-ion's transport. In contrast, for AF-LCO cycled upon pure CC procedure, not only the surface PTL thickness maintains ≈10 nm in whole 200 cycles, but also the subsurface structure always maintains a layered structure, as identified in Figure S5b-d (Supporting Information). The results indicate that, upon pure CC procedure, the surface phase structure of AF-LCO shows nearly no change since after the 1st cycle, which enables the well-functioned Li+-ion's transport across the surface structure with lesser capacity decay. Electrochemical impedance spectroscopy (EIS) plots are applied to clarify the Li⁺ ion's transport across the surface region of the AF-LCO, as shown in Figure S6 (Supporting Information). Two import parameters are fitted and compared, that is, the R_{CEL} and R_{ct} , among which, the R_{CEI} represents the CEI resistance, and the R_{ct} represents the charge transfer resistance of Li⁺ across the surface PTL.[26] We observe that, the main difference focuses on the $R_{\rm ct}$ values. The $R_{\rm ct}$ values of AF-LCO are obviously larger upon CC+CV procedure than that upon pure CC procedure, which is very consistent with the TEM results in Figure 5.

Besides the surface structure, the property of CEI layer also plays a significant role on enhancing the cycle stability of LCO.^[27] The CEI layers on AF-LCO surfaces upon CC+CV and pure

CC procedures are further characterized by TEM, as shown in Figure 6a,b, respectively. After the 200th cycle, a thick and loose CEI layer is observed on the AF-LCO surface with a thickness of beyond 100 nm upon CC+CV procedure, while for AF-LCO after the 200th cycle upon pure CC procedure, a thin and compact CEI layer is observed with a thickness of \approx 2 nm, which is \approx 50 times thinner than that upon CC+CV procedure. Since the CEI layer is formed through the electrode reactions between the cathode and electrolyte, it can be easily confirmed that the surface side reactions is much more severe upon CC+CV procedure than that upon pure CC procedure, mainly due to the CV charging. Thus, it is important to understand the CEI formation process upon cyclic CV charging process.

XPS analyses are utilized to detect the CEI composition at both fully charged and discharged states via analyzing the F 1s and O 1s spectra results, as shown in Figures S7 and S8 (Supporting Information). The F 1s peaks can be separated into three peaks, including Li_xFP_vO_z, LiAlF₄, and LiF, locating at binding energies of 686.6, 686.0, and 685.1 eV, respectively.[15a,17] Among the above inorganic components, the Li_xFP_vO_z comes from the decomposition of LiPF₆ salts, and the LiF is formed via both decomposition of the solvents and the PF₆⁻ anions.^[17,28] Table S1 (Supporting Information) shows the fitted contents of F-containing components in CEI, and the comparison of the LiF ratio in CEI

16163028, 2024, 14, Downloaded from https://advanced.onlinelibrary.wiley.com/doi/10.1002/adfm.202312837 by University Town Of Shenzhen, Wiley Online Library on [23/11/2025]. See the Terms

and Conditions

onditions) on Wiley Online Library for rules of use; OA articles are governed by the applicable Creative Commons

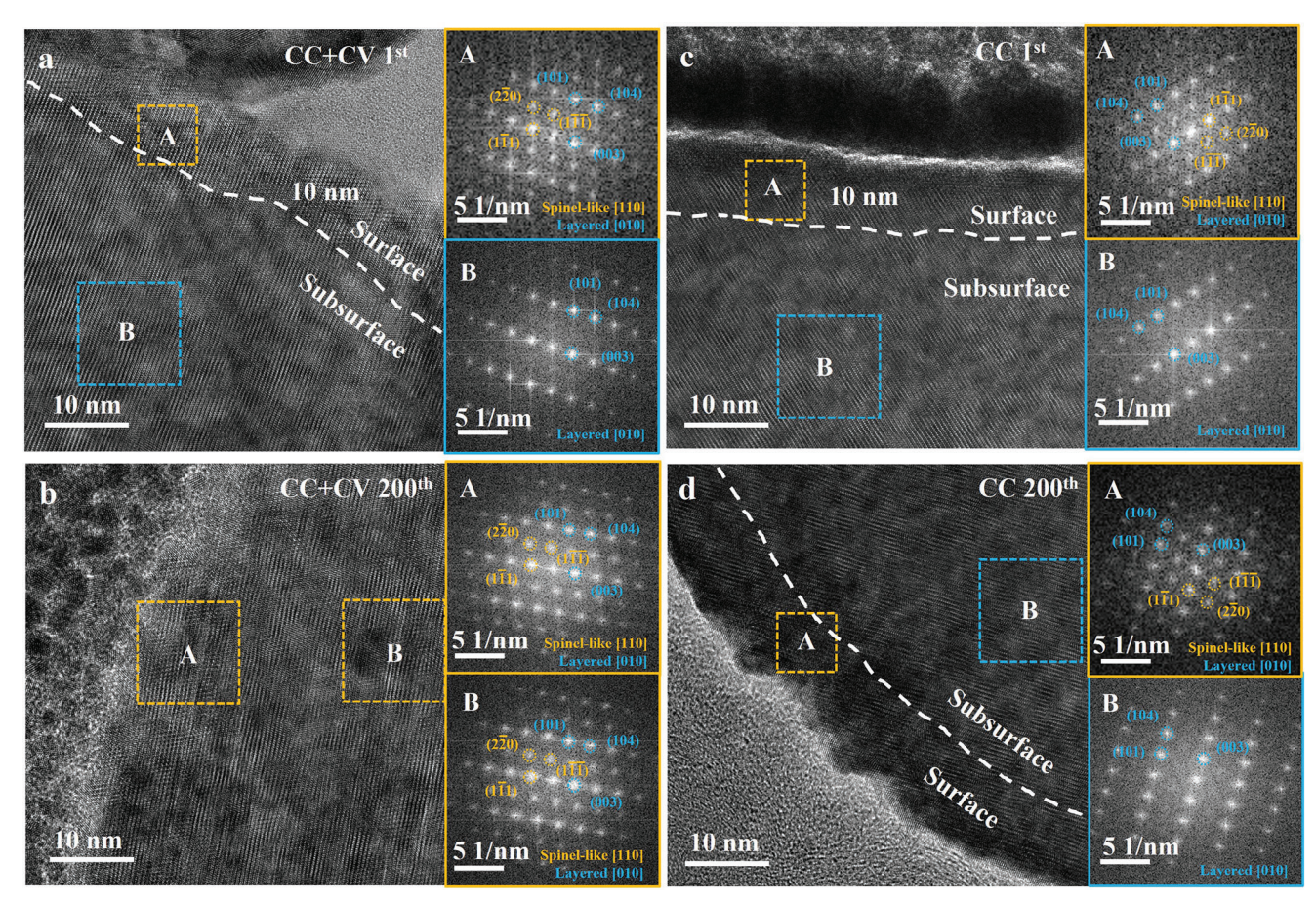


Figure 5. TEM characterizations on the surface structure deterioration of AF-LCO. a,b) The surface and subsurface structure features after the 1st cycle upon CC+CV and pure CC procedures, respectively. c,d) The surface and subsurface structure features after the 200th cycle upon CC+CV and pure CC procedures, respectively.

is shown in Figure 6c. We observed that, in the 1st cycle, the LiF in CEI layer is obviously higher at the discharged state than at the charged state. In other words, the LiF content in CEI gains upon discharging. A possible reaction path for this phenomenon can be clarified as follows: 1st, some solvents, such as EC, FEC, etc., are oxidized on AF-LCO surface upon charging, leading to the generation of some oxidation products, 2nd, upon discharging, part of the Li⁺ ions that migrates from the anode side can react with the above oxidation products, and result in the increase in LiF ratio in CEI layer.^[29] As the cycle proceeds, we find that the LiF in CEI at discharged state gradually increases upon CC+CV procedure, while it gradually decreases upon pure CC procedure. This result indicates that, the CV charging process in CC+CV procedure causes more oxidation of solvents, and then leads to more LiF generation upon discharging, which is one of the reasons for the accelerated capacity decay upon CC+CV procedure. As for pure CC procedure, the oxidation of solvents reduces after the 1st cycle, thus leading to the gradual decrease of LiF in CEI. Besides, the reduced oxidation of solvents further reduces the generation of HF, leading to the suppressed Co dissolution, therefore, the surface structure collapse can be greatly inhibited upon pure CC procedure.

The analyses of O 1s spectra results are shown in Figure S8 and Table S2 (Supporting Information). The O 1s peaks can be sepa-

rated into six peaks, including the lattice O, R-OLi, P-O, C-O, C=O, and Li_xFP_yO_z, locating at the binding energies of 529.8, 530.4, 531.2, 532.0, 532.9, and 534.1 eV, respectively.[30] We define the organic components in CEI as the sum of R-OLi, C-O, and C=O products, and the comparison of organic ratio in CEI is shown in Figure 6d. The result indicates that, the organic ratio in CEI upon CC+CV procedure is obviously larger than that upon pure CC procedure in 200 cycles, which further identify the aggregated oxidation of solvents. As previously reported, the aggregated oxidation of solvents can cause the increase of the electrolyte acidity via releasing the corrosive HF,[9a,b] which inevitably leads to more Co dissolution, as confirmed by the XPS Co 2p spectra results in Figure S9 (Supporting Information), in which obvious Co 2p signals are observed on the Li anode surface after 200 cycles upon the CC+CV procedure, while nearly no Co 2p signals can be detected on the Li anode upon the pure CC procedure. The more severe side reactions upon CC+CV procedure, including more solvents decomposition, more LiF generation, etc., can further lead to the lowered coulombic efficiency (CE) (Figure S10, Supporting Information). In summary, due to the surface structure deterioration caused by long-term cycling upon CC+CV procedure, including high R_{ct} caused by irreversible PTL and high $R_{\rm CEI}$ caused by accelerated CEI generation, the duration and capacity contribution of CV stage is prolonged

16163028, 2024, 14, Downloaded from https://advanced.onlinelibrary.wiley.com/doi/10.1002/adfm.202312837 by University Town Of Shenzhen, Wiley Online Library on [23/11/2025]. See the Terms and Conditions (https://onlinelibrary.wiley

and-conditions) on Wiley Online Library for rules of use; OA articles are governed by the applicable Creative Commons

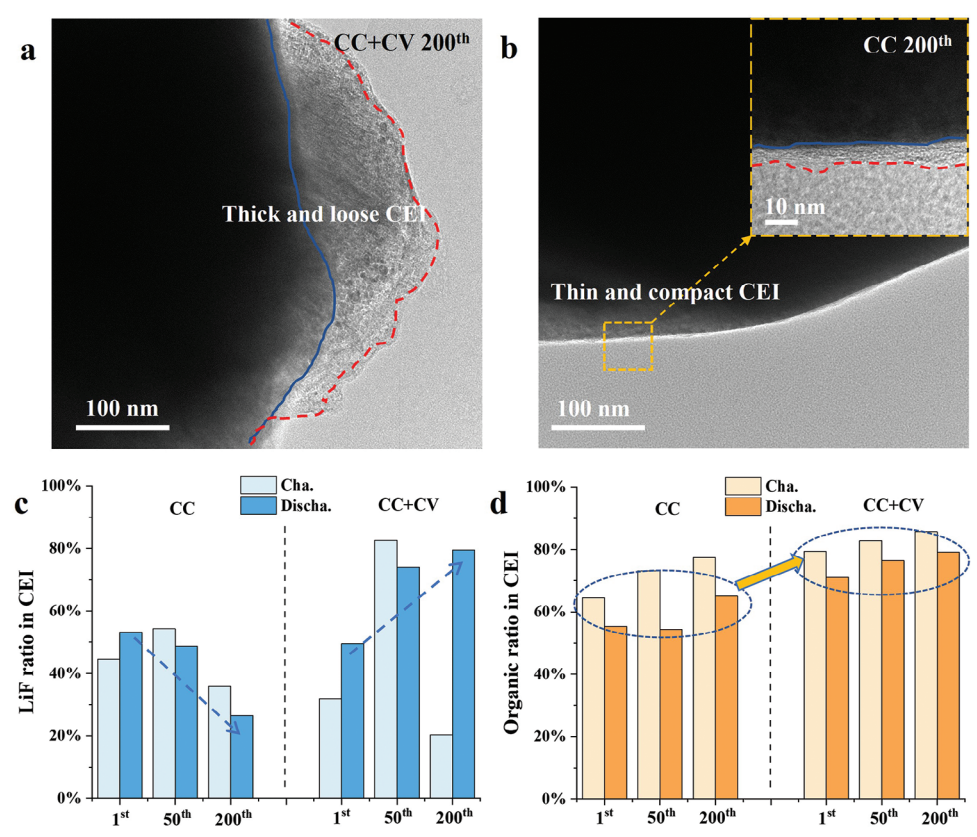


Figure 6. Characterizations of CEI. a,b) TEM characterizations of CEI layers on AF-LCO surface upon CC+CV and pure CC procedures. c,d) The ratio of LiF and organic components in CEI layers of AF-LCO after the 1st, 50th, and 200th cycles upon CC and CC+CV procedures, as fitted from the F 1s and O 1s spectra results.

(Figure S11, Supporting Information) as the cut-off current decreases.

After all, the structural stability of AF-LCO is systematically conducted to reveal the fading mechanism of the accelerated capacity decay upon CC+CV procedures, and the correlated schematic illustration for the structure deterioration is shown in **Figure 7**. Comparing with pure CC procedure, when the CV charging is introduced, the phase evolution upon charging causes more H1-3 phase separation, which is the origin of the structure damages, including the lattice dislocations, curved Co-O layers, and even the generation of microcracks in the bulk. These structure damages not only play a significant role on

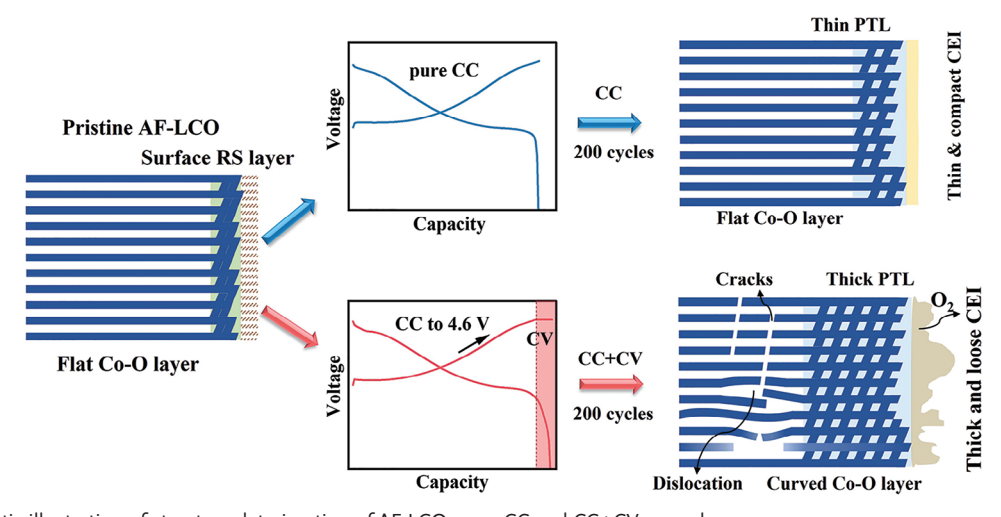


Figure 7. Schematic illustration of structure deterioration of AF-LCO upon CC and CC+CV procedures.



www.advancedsciencenews.com

___ MATERIALS

www.afm-journal.de

16163028, 2024, 14, Downloaded from https://advanced.onlinelibrary.wiley.com/doi/10.1002/adfm.202312837 by University Town Of Shenzhen, Wiley Online Library on [23/11/2025]. See the Terms and Conditions (https://advanced.onlinelibrary.wiley.com/doi/10.1002/adfm.202312837 by University Town Of Shenzhen, Wiley Online Library on [23/11/2025]. See the Terms and Conditions (https://advanced.onlinelibrary.wiley.com/doi/10.1002/adfm.202312837 by University Town Of Shenzhen, Wiley Online Library on [23/11/2025]. See the Terms and Conditions (https://advanced.onlinelibrary.wiley.com/doi/10.1002/adfm.202312837 by University Town Of Shenzhen, Wiley Online Library on [23/11/2025]. See the Terms and Conditions (https://advanced.onlinelibrary.wiley.com/doi/10.1002/adfm.202312837 by University Town Of Shenzhen, Wiley Online Library on [23/11/2025]. See the Terms and Conditions (https://advanced.onlinelibrary.wiley.com/doi/10.1002/adfm.202312837 by University Town Of Shenzhen, Wiley Online Library on [23/11/2025]. See the Terms and Conditions (https://advanced.onlinelibrary.wiley.com/doi/10.1002/adfm.202312837 by University Town Of Shenzhen, Wiley Online Library on [23/11/2025]. See the Terms and Conditions (https://advanced.onlinelibrary.wiley.com/doi/10.1002/adfm.202312837 by University Town Of Shenzhen, Wiley Online Library on [23/11/2025]. See the Terms and Conditions (https://advanced.onlinelibrary.wiley.com/doi/10.1002/adfm.202312837 by University Town Of Shenzhen, Wiley Online Library on [23/11/2025]. See the Terms and Conditions (https://advanced.onlinelibrary.wiley.com/doi/10.1002/adfm.202312837 by University Town Of Shenzhen, Wiley Online Library on [23/11/2025]. See the Terms and Conditions (https://advanced.onlinelibrary.wiley.com/doi/10.1002/adfm.202312837 by University Town Of Shenzhen, Wiley Online Library on [23/11/2025]. See the Terms and Conditions (https://advanced.onlinelibrary.wiley.com/doi/10.1002/adfm.20231281 by University (https://advanced.onlinelibrary.wiley.com/doi/10.1002/adfm.20231281 by University

and-conditions) on Wiley Online Library for rules of use; OA articles are governed by the applicable Creative Commons

blocking the Li⁺ ion's transport in the bulk, but also induce more side reactions through reacting with the penetrated electrolyte along the microcracks. From the surface structure aspect, the CV charging causes more "layer to spinel" phase transitions in the surface, leading to the formation of thick surface PTL upon cycle. The thick PTL layer increases the Li⁺ ion's transport resistance, or increases the value of R_{ct} . More importantly, the CV charging induces more side reactions, or more electrolyte decomposition. In one hand, the severe side reactions lead to the generation of thick and loose CEI with low protective ability, leading to the deteriorated CEI, lowered CE value, and prolonged CV charging time. And, the prolonged CV charging time in turn further promotes more side reactions, thus forms to an unwanted chain reaction for the accelerated capacity decay. On the other hand, the severe electrolyte decomposition can release more HF, leading to more Co dissolution, and more surface structure collapse issue, which seriously gains the charge transfer resistance and reduces the interface Li+ transport kinetics across the surface structure of AF-LCO.

3. Conclusion

In summary, we reveal the fading mechanism for the accelerated capacity decay of AF-LCO cycling upon a harsh CC+CV procedure at 3–4.6 V versus Li/Li⁺. Many characterizations are utilized, including the SEM, in situ and ex situ XRD, XPS, TEM, and electrochemical measurements, etc. The obtained results illustrate that the reasons for the accelerated capacity decay of AF-LCO under CC+CV procedure are as follows: 1st, the CV charging triggers more H1-3 phase separation, leading to the lattice dislocations, curved Co-O layers, and microcracks in bulk LCO regions; 2nd, the CV charging causes more side reactions and more surface structure collapse, which seriously gains the charge transfer resistance and reduces the Li⁺-ion's transport across the surface structure. This work provides a new insight into the fading mechanism of LCO, and shows significant guidance for the design of more practical LCO cathodes.

Supporting Information

Supporting Information is available from the Wiley Online Library or from the author.

Acknowledgements

Z.L. and H.Y. contributed equally to this work. This work was financially supported by the National Natural Science Foundation of China (52102201), and the major science and technology infrastructure project of material genome big-science facilities platform supported by the municipal development and reform commission of shenzhen.

Conflict of Interest

The authors declare no conflict of interest.

Data Availability Statement

The data that support the findings of this study are available from the corresponding author upon reasonable request.

Keywords

charging procedure, fading mechanism, LiCoO₂, phase evolution, side reaction

> Received: October 17, 2023 Revised: November 26, 2023 Published online: December 27, 2023

- [1] a) K. Mizushima, P. C. Jones, P. J. Wiseman, J. B. Goodenough, *Mater. Res. Bull.* 1980, 15, 783; b) Y. J. Kim, J. Cho, T.-J. Kim, B. Park, J. Electrochem. Soc. 2003, 150, A1723.
- [2] Y. Kim, G M. Veith, J. Nanda, R R. Unocic, M. Chi, N J. Dudney, Electrochim. Acta 2011, 56, 6573.
- [3] a) Y. Huang, Y. Zhu, H. Fu, M. Ou, C. Hu, S. Yu, Z. Hu, C-Te Chen, G. Jiang, H. Gu, He Lin, W. Luo, Y. Huang, Angew. Chem. Int. Ed. 2021, 60, 4682; b) L. Wang, J. Ma, C. Wang, X. Yu, R. Liu, F. Jiang, X. Sun, A. Du, X. Zhou, G. Cui, Adv. Sci. 2019, 6, 1900355.
- [4] a) J.-N. Zhang, Q. Li, C. Ouyang, X. Yu, M. Ge, X. Huang, E. Hu, C. Ma, S. Li, R. Xiao, W. Yang, Y. Chu, Y. Liu, H. Yu, X.-Q. Yang, X. Huang, L. Chen, H. Li, Nat. Energy 2019, 4, 594; b) A. Fu, Z. Zhang, J. Lin, Y. Zou, C. Qin, C. Xu, P. Yan, K. Zhou, J. Hao, X. Yang, Y. Cheng, D.-Y. Wu, Y. Yang, M.-S. Wang, J. Zheng, Energy Storage Mater. 2022, 46, 406.
- [5] M. Duffiet, M. Blangero, P.-E. Cabelguen, C. Delmas, D. Carlier, J. Phys. Chem. Lett. 2018, 9, 5334.
- [6] A. Yano, M. Shikano, A. Ueda, H. Sakaebe, Z. Ogumi, J. Electrochem. Soc. 2017, 164, A6116.
- [7] a) J. Chen, H. Chen, S. Zhang, A. Dai, T. Li, Yu Mei, L. Ni, Xu Gao, W. Deng, L. Yu, G. Zou, H. Hou, M. Dahbi, W. Xu, J. Wen, J. Alami, T. Liu, K. Amine, X. Ji, Adv. Mater. 2022, 34, 2204845; b) T. Fan, W. Kai, V. K. Harika, C. Liu, A. Nimkar, N. Leifer, S. Maiti, J. Grinblat, M. N. Tsubery, X. Liu, M. Wang, L. Xu, Y. Lu, Y. Min, N. Shpigel, D. Aurbach, Adv. Funct. Mater. 2022, 32, 2204972; c) S. Mao, Z. Shen, W. Zhang, Q. Wu, Z. Wang, Y. Lu, Adv. Sci. 2022, 9, 2104841; d) S. Ding, M. Zhang, R. Qin, J. Fang, H. Ren, H. Yi, L. Liu, W. Zhao, Y. Li, Lu Yao, S. Li, Q. Zhao, F. Pan, Nano-Micro Lett. 2021, 13, 173.
- [8] X. Tan, Y. Zhang, S. Xu, P. Yang, T. Liu, D. Mao, J. Qiu, Z. Chen, Z. Lu, F. Pan, W. Chu, Adv. Energy Mater. 2023, 13, 2300147.
- [9] a) D. Aurbach, B. Markovsky, A. Rodkin, E. Levi, Y. S Cohen, H.-J Kim, M. Schmidt, Electrochim. Acta 2002, 47, 4291; b) M. Hirooka, T. Sekiya, Y. Omomo, M. Yamada, H. Katayama, T. Okumura, Y. Yamada, K. Ariyoshi, Electrochim. Acta 2019, 320, 134596; c) Yi Wang, Q. Zhang, Z.-C. Xue, L. Yang, J. Wang, F. Meng, Q. Li, H. Pan, J.-N. Zhang, Z. Jiang, W. Yang, X. Yu, L. Gu, H. Li, Adv. Energy Mater. 2020, 10, 2001413; d) Y. Yan, Y. Zheng, H. Zhang, J. Chen, G. Zeng, L. Wang, B. Zhang, S. Zhou, Y. Tang, A. Fu, L. Zheng, H. Huang, Y. Zou, C.-W. Wang, X. Kuai, Y. Sun, Yu Qiao, S.-G. Sun, Adv. Funct. Mater. 2023, 33, 2304496.
- [10] a) S. Erol, M E. Orazem, R P. Muller, J. Power Sources 2014, 270, 92; b)
 E. Zhitao, H. Guo, G. Yan, J. Wang, R. Feng, Z. Wang, X. Li, J. Energy Chem. 2021, 55, 524; c) J. Oh, S.-Y. Lee, H. Kim, J. Ryu, B. Gil, J. Lee, M. Kim, Adv. Sci. 2022, 9, 2203639.
- [11] G. Sun, Fu-Da Yu, Mi Lu, Q. Zhu, Y. Jiang, Y. Mao, J A. Mcleod, J. Maley, J. Wang, J. Zhou, Z. Wang, Nat. Commun. 2022, 13, 6464.
- [12] a) K. Guo, C. Zhu, H. Wang, S. Qi, J. Huang, D. Wu, J. Ma, Adv. Energy Mater. 2023, 13, 2204272; b) M. Hirooka, T. Sekiya, Y. Omomo, M. Yamada, H. Katayama, T. Okumura, Y. Yamada, K. Ariyoshi, J. Power Sources 2020, 463, 228127; c) W. Pu, Y. Meng, Y. Wang, Y. Ge, X. Li, P. Wang, Z. Zhang, Y. Guo, D. Xiao, ACS Appl. Energy Mater. 2021, 4, 6933; d) Z. Zhang, Y. Meng, D. Xiao, Energy Stor. Mater. 2023, 56, 443



www.advancedsciencenews.com



www.afm-journal.de

16163028, 2024, 14, Downloaded from https://advanced.onlinelibrary.wiley.com/doi/10.1002/adfm.202312837 by University Town Of Shenzhen, Wiley Online Library on [23/11/2025]. See the Terms

and Conditions

and-conditions) on Wiley Online Library

of use; OA articles are governed by the applicable Creative Commons

- [13] Z. Li, H. Yi, H. Ren, J. Fang, Y. Du, W. Zhao, H. Chen, Q. Zhao, F. Pan, Adv. Funct. Mater. 2023, 33, 2307913.
- [14] H. Yi, Y. Du, J. Fang, Z. Li, H. Ren, W. Zhao, H. Chen, L. Zhou, Q. Zhao, F. Pan, ACS Appl. Mater. Interfaces 2023, 15, 42667.
- [15] a) J. Qian, L. Liu, J. Yang, S. Li, X. Wang, H L. Zhuang, Y. Lu, Nat. Commun. 2018, 9, 4918; b) W. Huang, Q. Zhao, M. Zhang, S. Xu, H. Xue, C. Zhu, J. Fang, W. Zhao, G. Ren, R. Qin, Q. Zhao, H. Chen, F. Pan, Adv. Energy Mater. 2022, 12, 2200813.
- [16] S. Xu, X. Tan, W. Ding, W. Ren, Qi Zhao, W. Huang, J. Liu, R. Qi, Y. Zhang, J. Yang, C. Zuo, H. Ji, H. Ren, Bo Cao, H. Xue, Z. Gao, H. Yi, W. Zhao, Y. Xiao, Q. Zhao, M. Zhang, F. Pan, *Angew. Chem. Int. Ed.* 2023, 62, 202218595.
- [17] Yi-C Lu, A N. Mansour, N. Yabuuchi, Y. Shao-Horn, Chem. Mater. 2009. 21, 4408.
- [18] A. Yano, N. Taguchi, H. Kanzaki, M. Shikano, H. Sakaebe, J. Electrochem. Soc. 2021, 168, 050517.
- [19] He Huang, Z. Li, S. Gu, J. Bian, Y. Li, J. Chen, K. Liao, Q. Gan, Y. Wang, S. Wu, Z. Wang, W. Luo, R. Hao, Z. Wang, G. Wang, Z. Lu, Adv. Energy Mater. 2021, 11, 2101864.
- [20] a) B. Hu, X. Lou, C. Li, F. Geng, C. Zhao, J. Wang, M. Shen, B. Hu, J. Power Sources 2019, 438, 226954; b) Z. Chen, J. R. Dahn, Electrochim. Acta 2004, 49, 1079.
- [21] C.-W. Wang, S.-J. Zhang, C. Lin, S. Xue, Ya-P Deng, B. Zhang, L. Yang, X. Yao, L. Zeng, J.-T. Li, F. Pan, Zu-W Yin, *Nano Energy* 2023, 108, 108192.
- [22] J. Li, C. Lin, M. Weng, Yi Qiu, P. Chen, K. Yang, W. Huang, Y. Hong, J. Li, M. Zhang, C. Dong, W. Zhao, Z. Xu, Xi Wang, K. Xu, J. Sun, F. Pan, Nat. Nanotechnol. 2021, 16, 599.
- [23] a) H. Ren, W. Zhao, H. Yi, Z. Chen, H. Ji, Qi Jun, W. Ding, Z. Li, M. Shang, J. Fang, Ke Li, M. Zhang, S. Li, Q. Zhao, F. Pan, Adv. Funct.

- Mater. 2023, 33, 2302622; b) D. Takamatsu, Y. Koyama, Y. Orikasa, S. Mori, T. Nakatsutsumi, T. Hirano, H. Tanida, H. Arai, Y. Uchimoto, Z. Ogumi, Angew. Chem., Int. Ed. 2012, 51, 11597.
- [24] a) X. Tan, T. Zhao, L. Song, D. Mao, Y. Zhang, Z. Fan, H. Wang, W. Chu, Adv. Energy Mater. 2022, 12, 2200008; b) Y. Ma, Mu Chen, Y. Yan, Y. Wei, W. Liu, X. Zhang, J. Li, Z. Fu, J. Li, X. Zhang, J. Mater. Res. 2020, 35, 31.
- [25] T. Liu, J. Liu, L. Li, L. Yu, J. Diao, T. Zhou, S. Li, A. Dai, W. Zhao, S. Xu, Y. Ren, L. Wang, T. Wu, R. Qi, Y. Xiao, J. Zheng, W. Cha, R. Harder, I. Robinson, J. Wen, J. Lu, F. Pan, K. Amine, *Nature* 2022, 606, 305
- [26] a) W. Hu, Y. Peng, Y. Wei, Y. Yang, J. Phys. Chem. C. 2023, 127, 4465; b)
 B. Zhang, L. Wang, Y. Zhang, X. Wang, Yu Qiao, S.-G. Sun, J. Chem. Phys. 2023, 158, 054202; c) Q. Zhao, A. Song, W. Zhao, R. Qin, S. Ding, X. Chen, Y. Song, L. Yang, H. Lin, S. Li, F. Pan, Angew. Chem., Int. Ed. 2021, 60, 4169.
- [27] a) Y. Qin, K. Xu, Q. Wang, M. Ge, T. Cheng, M. Liu, H. Cheng, Y. Hu, C. Shen, D. Wang, Y. Liu, B. Guo, *Nano Energy* **2022**, *96*, 107082; b) J. Zhang, P.-F. Wang, P. Bai, H. Wan, S. Liu, S. Hou, X. Pu, J. Xia, W. Zhang, Z. Wang, Bo Nan, X. Zhang, J. Xu, C. Wang, *Adv. Mater.* **2022**, *34*, 2108353.
- [28] M. Mao, B. Huang, Q. Li, C. Wang, Y.-B. He, F. Kang, Nano Energy 2020, 78, 105282.
- [29] J.-N. Zhang, Q. Li, Y. Wang, J. Zheng, X. Yu, H. Li, Energy Storage Mater. 2018, 14, 1.
- [30] a) Yi Wang, Q. Zhang, Z.-C. Xue, L. Yang, J. Wang, F. Meng, Q. Li, H. Pan, J.-N. Zhang, Z. Jiang, W. Yang, X. Yu, L. Gu, H. Li, Adv. Energy Mater. 2020, 10, 2001413; b) R. Qin, S. Ding, C. Hou, L. Liu, Y. Wang, W. Zhao, Lu Yao, Y. Shao, R. Zou, Q. Zhao, S. Li, F. Pan, Adv. Energy Mater. 2023, 13, 2203915.